COMMUNICATION

Electronic Properties at Gold/Conjugated-Polyelectrolyte Interfaces

By *Jung Hwa Seo, Renqiang Yang, Jacek Z. Brzezinski, Bright Walker, Guillermo C. Bazan,* and Thuc-Quyen Nguyen**

Interest in conjugated polyelectrolytes (CPEs) has grown in recent years due to their applications in polymer light-emitting diodes (PLEDs),[1–2] polymer solar cells,[3] and optically amplified biosensor assays.[4] Introducing CPEs into optoelectronic devices offers new fabrication opportunities and functions.[5] From a practical perspective, their solubility in polar solvents allows integration within multilayer devices using solution-casting methods.[1] More importantly, CPEs were recently found to be efficient electron-transport layers (ETLs) in PLEDs that incorporate high-work-function (WF) cathodes. It has also been previously reported that the performance of such PLEDs is strongly influenced by the backbone structure and charge-compensating counterions.[1,6] Proposed mechanisms for the reduction of change injection barriers include the introduction of a self-assembled interfacial dipole (which shifts the vacuum level (VL)) and ion migration (which screens the field at the interfaces). Although structure–function relationships in PLEDs have been studied by modifications of polymer structure,[7] the counterion effect on electrical properties of CPEs at metallic interfaces remains to be fully understood.

A complete picture for understanding the performance of optoelectronic devices requires the electronic structure at polymer/electrode interfaces. X-ray and UV photoelectron spectroscopy (XPS and UPS, respectively) are widely used to determine such energy-level alignments. XPS probes the core energy levels, and thereby gives insight into any chemical reaction, as well as the band bending, caused by equilibration of the different Fermi levels (E_F) on both sides of the interface.[8–10] For example, if the WF of the metal is higher than that of the organic layer, electron density moves into the metal from the organic layer, until the E_F is equilibrated. Therefore, the band bending is an important parameter to determine charge-carrier injection barriers in real devices containing thick organic layers.[8a,10] UPS is used to determine the WF of a metal and the VL and highest occupied molecular orbital (HOMO) positions of organic semiconductors.[8,9] When an organic solid contacts a metal, the organic layer may be affected by the potential of the surface dipole. The VL shifts can yield the magnitude and direction of the interfacial dipole (Δ). Generally, a downward shift of VL ($\Delta < 0$) gives rise to a larger hole-injection barrier (ϕ_h), while an upward shift ($\Delta > 0$) provides a larger electron-injection barrier (ϕ_e).[8–10]

XPS and UPS studies are typically carried out by growing organic thin films of progressive thicknesses atop a metallic surface or a single crystal.[11] These films are usually deposited in several steps, and are subsequently analyzed without breaking the vacuum.[8–12] In contrast, polymers are nonvolatile, and are therefore commonly processed from solution by methods that do not offer as good a control over layer thickness.[13] Most polymer/metal interfaces have been studied by evaporating the metal in situ on ex-situ-prepared films.[14] Examples of the reverse procedure are scarce.[15]

In this contribution, we investigate the electronic structures of one neutral conjugated polymer and three CPEs using XPS and UPS. Control of film thickness was achieved by varying the spin-casting speed and the solution concentration. As shown in Scheme 1, the materials studied are poly[9,9-bis[6′-(*N,N,N*-trimethylammonium)hexyl]fluorene-*alt-co*-1,4-phenylene]bromide (**PFN$^+$Br$^-$**), poly[9,9-bis(6′-bromohexyl)fluorene-*alt-co*-1,4-phenylene] (**PFN-Br**), poly[9,9-bis[6′-(*N,N,N*-trimethylammonium)-hexyl] fluorene-*alt-co*-1,4-phenylene] tetrakis (imidazoly)borate (**PFN$^+$BIm$_4^-$**), and sodium poly[9,9-bis(4′-surfonatobutyl) fluorine-*alt-co*-1,4-phenylene] (**PFNSO$_3^-$Na$^+$**). The manuscript is organized as follows. First, we provide details on film preparation and the analysis of XPS and UPS data. The results on **PFN-Br**/Au are then used as an example to guide the reader on how the basic electronic parameters are determined. Spectral characteristics of the other three polymers are subsequently described in less detail. The manuscript concludes by providing a complete picture of the electronic properties at the Au interface as a function of CPE structure.

Polymers were deposited by spin coating from a suitable solvent and at an appropriate spin speed (Experimental Section). Film thickness was determined by a combination of atomic force microscopy (AFM) and XPS measurements (Supporting Information). From the XPS and UPS spectra, the molecular orbital alignment, Δ, and band bending at the interface are determined according to the following equations:[8–11]

$$\mathrm{WF} = h\nu - E_{\mathrm{SE}} \quad (1)$$

$$\mathrm{IP} = h\nu - (E_{\mathrm{SE}} - E_{\mathrm{HOMO}}) \quad (2)$$

$$E_{\mathrm{LUMO}} = E_{\mathrm{g}} - E_{\mathrm{HOMO}} \quad (3)$$

$$\mathrm{EA} = \phi_{\mathrm{polymer}} - E_{\mathrm{LUMO}} \quad (4)$$

[*] Prof. G. C. Bazan, Prof. T.-Q. Nguyen, Dr. J. H. Seo, Dr. R. Yang, Dr. J. Z. Brzezinski, B. Walker
Center of Polymers and Organic Solids
Department of Chemistry and Biochemistry
University of California at Santa Barbara
Santa Barbara, CA 93106 (USA)
E-mail: bazan@chem.ucsb.edu; quyen@chem.ucsb.edu

DOI: 10.1002/adma.200802420

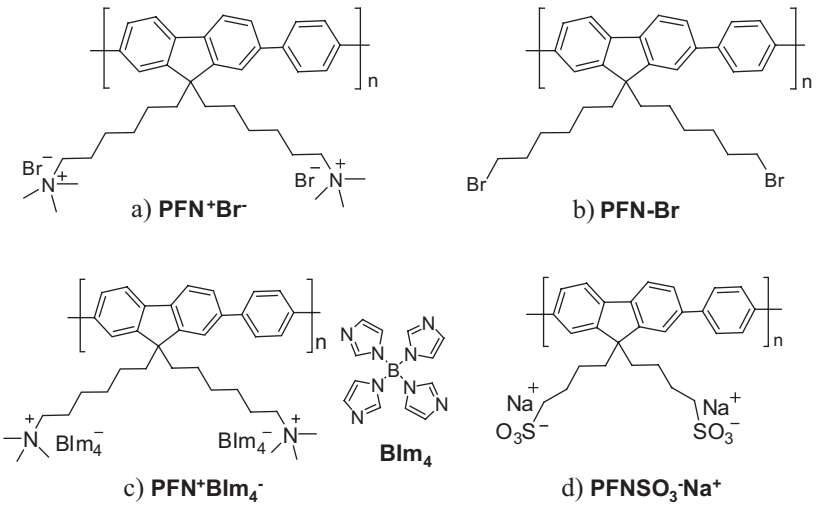

Scheme 1. Chemical structures of a neutral conjugated polymer and three CPEs, a) **PFN$^+$Br$^-$**, b) **PFN-Br**, c) **PFN$^+$BIm$_4^-$**, and d) **PFNSO$_3^-$Na$^+$**.

$$\Delta = \phi_{\text{polymer}} - \phi_{\text{Au}} + V_{\text{b}} \quad (5)$$

where $h\nu$ is the incident photon energy, E_{SE} is the secondary edge position, E_{HOMO} is the onset energy of the HOMO level, E_{g} is the optical band gap, E_{LUMO} is the energy of the lowest unoccupied molecular orbital (LUMO) level, ϕ_{Poymer} is the WF of the final polymer overlayer, ϕ_{Au} is the WF value of the Au surface, and V_{b} is the band-bending shift.

Figure 1 illustrates the procedure for the determination of energy-level alignment at the interfaces. Typical UPS spectra of a polymer (filled circles, top) and Au (solid line, bottom) are shown in Figure 1a. An energy diagram constructed using the above equations is displayed in Figure 1b. The WF value is determined by subtracting E_{SE} from $h\nu$. The ionization potential (IP) is determined using E_{SE}, $h\nu$, and E_{HOMO}, as determined by UPS. The Δ can be determined from the difference between ϕ_{Au} and ϕ_{Poymer}, together with V_{b}. E_{LUMO} was estimated using the known E_{g} value.[13b] Finally, the electron affinity (EA) was derived by subtracting E_{LUMO} from ϕ_{Poymer}.[8–15]

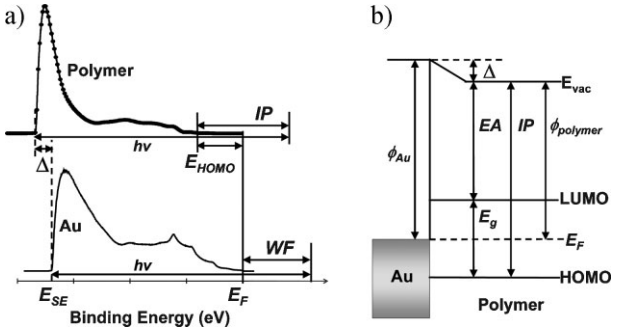

Figure 1. Schematic presentation for determination of energy level alignment at a polymer/Au interface. a) UPS spectra of a polymer (filled circle line, top) and of an Au layer (solid line, bottom). b) An energy-level diagram to illustrate the quantities in Equations 1–5.

Figure 2a and b show the C 1s and Br 3d emission lines from the **PFN-Br** layers as a function of film thickness, as obtained by XPS. The bottom of Figure 2a shows a weak C 1*s* peak at 284.2 eV from the Au surface, indicating a small amount of unavoidable hydrocarbon contamination.[15] No significant oxygen-related emission was detected in any of the samples examined. As the **PFN-Br** thickness increases to 22 nm, the C 1s and Br 3d emissions increase in intensity, while the Au 4*f* emissions become attenuated due to the thicker **PFN-Br** layers. No evidence of a chemical reaction is detected from the C 1s, Br 3d, and Au 4f emission lines (see Fig. S2 in the Supporting Information). Therefore, we suggest that the Au surface remains chemically intact, and gives rise to no band bending in the metal. Similar trends were also observed

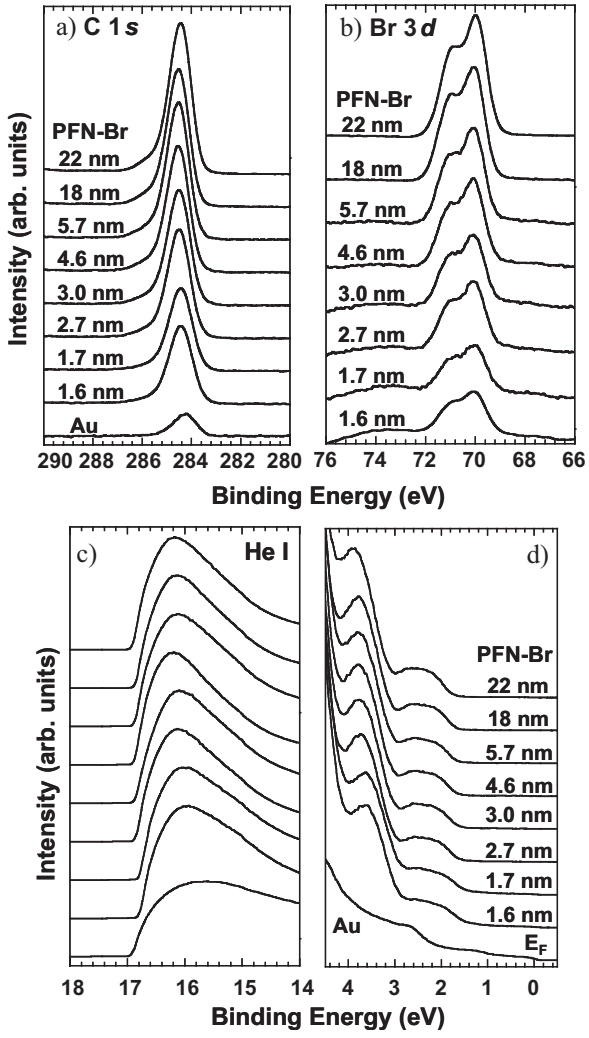

Figure 2. The evolution of XPS a) C 1s, b) Br 3d core levels of **PFN-Br** films with increasing **PFN-Br** thickness. UPS spectra of c) the secondary edge region and d) the HOMO region of **PFN-Br** with increasing **PFN-Br** thickness.

for other CPEs. With a 1.6 nm **PFN-Br** layer, the C 1s and Br 3d core levels are 284.4 and 70 eV, respectively. The C 1*s* structure consists of at least three emission lines, which are assigned as follows: 284.4 eV for aromatic carbons, ~285 eV for CH_2 chains, and the shoulder at 286 eV for C–Br bonds.[16,17] The Br 3d core level is consistent with the presence of C–Br bonds.[18,19] A slight shift of the C 1s and Br 3d peaks is observed up to 3 nm thickness, after which there is no further change, consistent with little or no band bending.

Figure 2c and d show UPS spectra taken for the **PFN-Br** films. E_F was determined from the Au surface, and all other spectra are plotted with respect to this value. In other words, the abscissa is the binding energy relative to the E_F of Au. The normalized secondary edges of **PFN-Br** are shown in Figure 2c. The VLs of the samples were determined by linear extrapolation of secondary electron cutoffs on the high-binding-energy side of the UPS spectra (14–18 eV). The secondary edges shift toward lower binding energies for the first two samples. As the **PFN-Br** layer becomes thicker after the third sample, the secondary edges shift toward higher binding energies. The final secondary edge is assigned to the 22 nm **PFN-Br** spectrum. The **PFN-Br** VL ($E_{SE} = 16.82$ eV) is only 0.02 eV higher than that of the Au surface ($E_{SE} = 16.84$ eV), thus the VL shift is negligible at the interface. Figure 2d also shows the evolution of the HOMO onsets for **PFN-Br**. The Au peak is completely suppressed by the **PFN-Br** emission when the film thickness is greater than 3 nm, indicating a continuous film. Comparing the shift in the HOMO onset in the 22 nm film (1.74 eV) to the E_F of Au provides the relative position of the HOMO level.

The peak shifts of the C 1s and Br 3d lines are summarized in Figure 3a, where the positions are plotted versus the layer thickness. Peak shifts are calculated relative to the first deposition sample. One can see that the C 1s peaks have a similar trend to the Br 3d peaks. The WF and IP of the sample surface values versus thickness presented in Figure 3b show little variation. From the absence of change in the C 1s and Br 3d peaks, and the slight shift of secondary edge, it can be surmised that the electronic structure at the **PFN-Br**/Au interface exhibits very little Δ and band bending. Figure 3 also contains results from the other CPEs, which will be discussed subsequently, so that relative comparisons can be readily made.

The properties of the anionic CPE, **$PFNSO_3^-Na^+$**, are discussed next. Figure 4a shows that the C 1s emission lines become more intense as the thickness increases, as is the case for other core levels (O 1s, Na 2s, and S 2p). The C 1s peaks from a 1.7 nm layer exhibit a fairly distinct maximum at 284.75 eV, indicating a different chemical environment with the neutral **PFN-Br**. The total C 1s peak shift was 0.05 eV toward a higher binding energy after a sufficient coverage of **$PFNSO_3^-Na^+$** (27 nm), and is consistent with those measured from other core

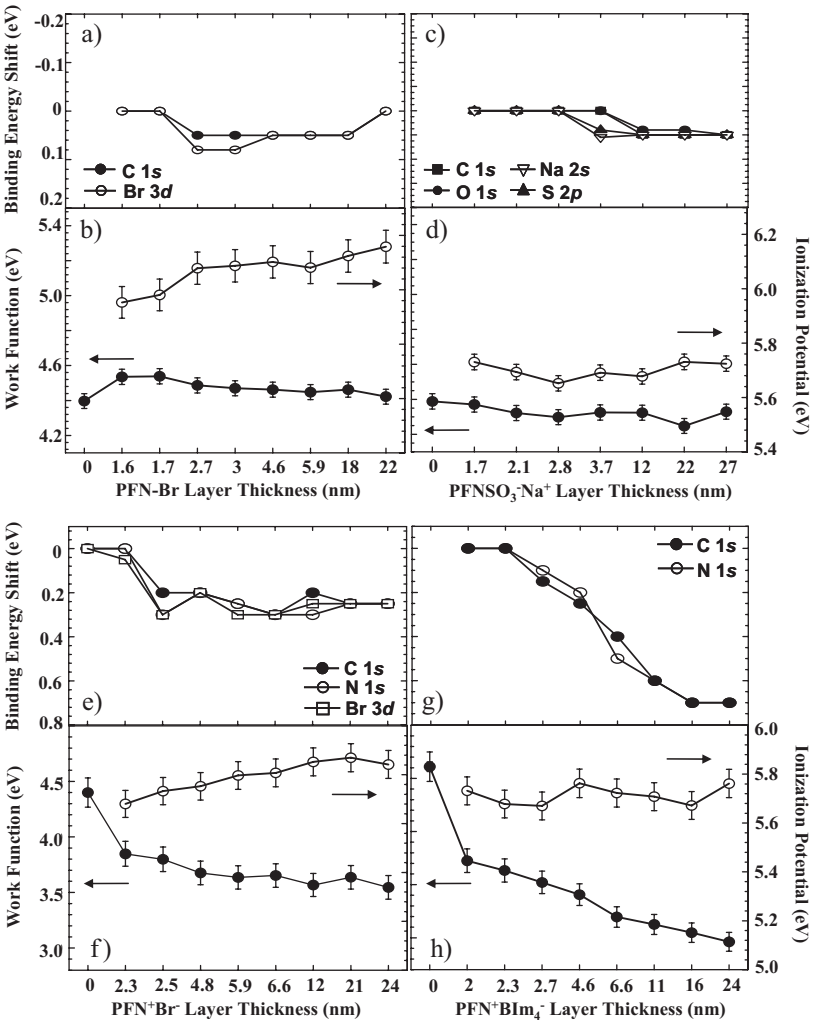

Figure 3. Binding energy shifts of XPS core levels versus a) **PFN-Br**, c) **$PFNSO_3^-Na^+$**, e) **PFN^+Br^-**, and g) **$PFN^+BIm_4^-$** layer thickness, respectively. Changes of the WF and IP in the b) **PFN-Br**, d) **$PFNSO_3^-Na^+$**, f) **PFN^+Br^-**, and h) **$PFN^+BIm_4^-$**, respectively.

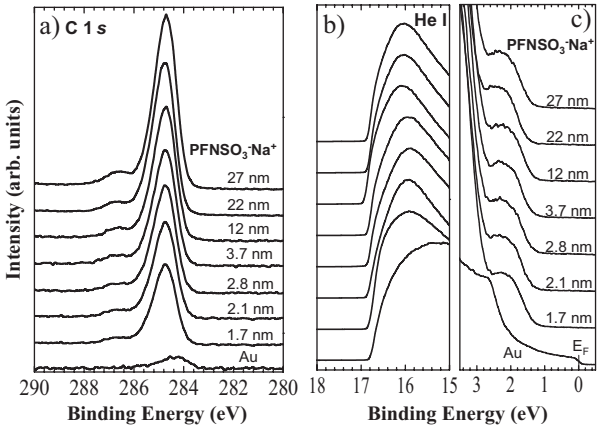

Figure 4. The evolution of XPS a) C 1s and UPS spectra of b) the secondary edge region and c) the HOMO region of **$PFNSO_3^-Na^+$** with increasing **$PFNSO_3^-Na^+$** thickness.

levels. From the peak shifts of all component lines summarized in Figure 3c, it can be determined that the magnitude of the band bending at the **PFNSO$_3^-$Na$^+$**/Au interface is 0.05 eV.

UPS spectra of **PFNSO$_3^-$Na$^+$** layers and a bare Au layer are shown in Figure 4b and c. The secondary edge shows negligible changes up to 3.7 nm, indicating the absence of a dipole shift. The total shift of the secondary edge ($E_{SE} = 16.88$ eV) for the 27 nm layer is 0.04 eV toward higher binding energy from that of Au. The corresponding HOMO level is therefore estimated to be 1.39 eV relative to E_F. The fact that Figure 3d shows little change in WF and IP as a function of **PFNSO$_3^-$Na$^+$** thickness indicates that the Δ and band bending at the **PFNSO$_3^-$Na$^+$**/Au interface are negligible, as observed with **PFN-Br**.

We now examine the first example of a cationic CPE structure. Figure 5a–c show emission lines from **PFN$^+$Br$^-$**. In contrast to **PFN-Br**, the C 1s emissions consist of two peaks, reflecting photoemissions from hydrocarbons and aromatic carbons in the main peak (285 eV) and from C–N bonds at ~286.7 eV. The Br 3d core level of 67.7 eV for the 2.3 nm layer is different from that observed with **PFN-Br** (see Fig. 2b), and corresponds to the ionic state of Br.[17] The N 1s core level at 403.3 eV is consistent with quaternized N–C functionalities.[16a,18] In contrast to **PFN-Br** and **PFNSO$_3^-$Na$^+$**, a shift in the C 1s peak of 0.25 eV toward higher binding energies for **PFN$^+$Br$^-$** is observed in the 24 nm layer. Furthermore, because the general shape of the peak does not change, we suggest the absence of a chemical reaction at the **PFN$^+$Br$^-$**/Au interface. Band bending thus leads to a 0.25 eV shift in the N 1s, C 1s, and Br 3d peaks (Fig. 3e).

The UPS spectra of **PFN$^+$Br$^-$** are provided in Figure 5d and e. The total VL shift and the HOMO level at the saturated coverage (24 nm) are 0.73 and 2.18 eV, respectively. Combining these data with the XPS results allows us to generate Figure 3f, which provides IP and WF as function of film thickness. The WF and core level shifts show similar shapes at their start and end points, and deviate significantly in the intermediate region, where band bending evolves. The steep change of WF between Au and the 2.3 nm layer stems from the secondary edge shift upon the deposition of the first layer. Comparison between the curves yields that the WF changes more rapidly than the XPS peak shifts. This can be explained by the fact that the C 1s (and also N 1s and Br 3d) emissions represent an average over the volume below the sample surface, covered by the escape depth of the photoelectrons.

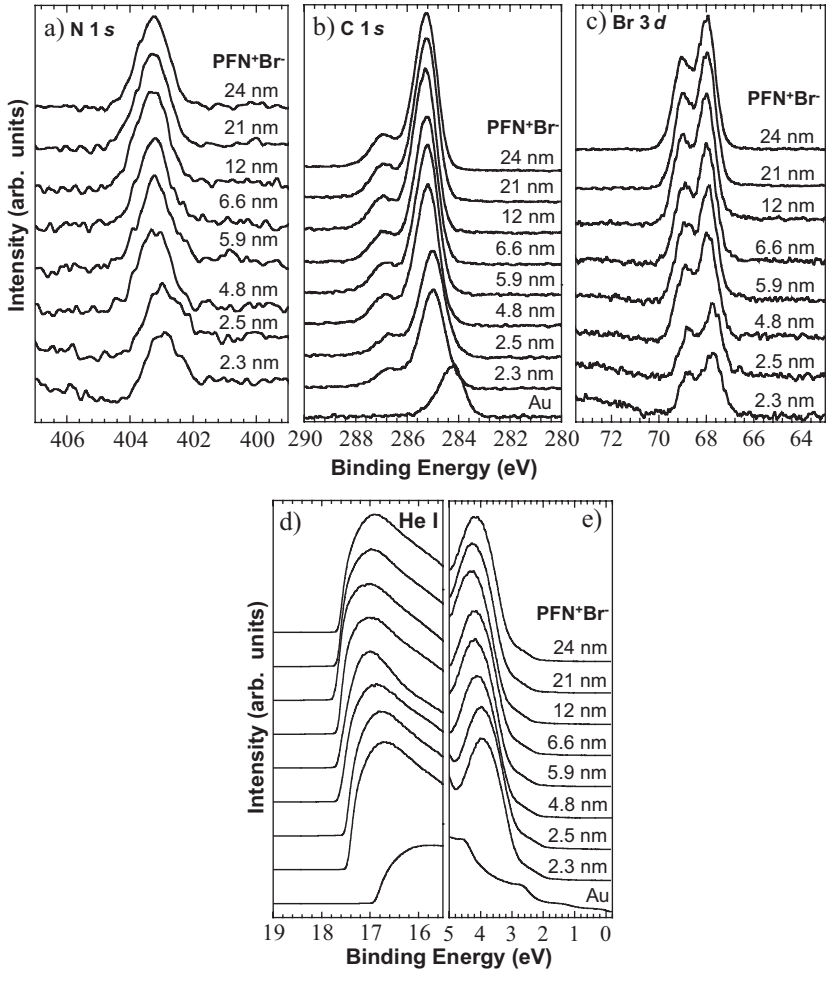

Figure 5. The XPS spectra of a) N 1s, b) C 1s, and Br 3d core levels of **PFN$^+$Br$^-$** films with increasing **PFN$^+$Br$^-$** thickness. UPS spectra of d) the secondary edge region and e) the HOMO region of **PFN$^+$Br$^-$** with increasing **PFN$^+$Br$^-$** thickness.

Examination of **PFN$^+$BIm$_4^-$** and comparison of the results obtained with **PFN$^+$Br$^-$** gives insight into the influence of the charge-compensating anion with a given cationic CPE backbone. XPS data obtained from **PFN$^+$BIm$_4^-$** as a function of layer thickness are shown in Figure 6a and b. The N 1s structure consists of at least three emission lines, which correspond to 399.3 and 400.3 eV for nitrogen bonds in the **BIm$_4$** ligands and 403.4 eV for the quaternized –N–CH$_3$ groups.[18] Among these polymers, a remarkable shift in the C 1s peak, of 0.7 eV toward higher binding energies for **PFN$^+$BIm$_4^-$**, is observed in the 24 nm layer. UPS spectra of the **PFN$^+$BIm$_4^-$** films on Au surface are presented in Figure 6c and d. The most significant feature is a continuous 1.43 eV shift of the secondary edges toward higher binding energies with increasing thickness (Fig. 3g), which implies that the VL is lower compared to that of the Au and the presence of an interfacial dipole. Figure 3h summarizes the WF and IP changes. The total WF change coincides with the N 1s and C 1s peak curves. The WF change is thus closely connected to band bending at the interface. The IP has almost a constant value in the range of $\pm$0.05 eV.

Energy diagrams for the neutral conjugated polymer and three CPEs can therefore be generated by combining the XPS and UPS data discussed above, as shown in Figure 7. The charged polymers have different electronic properties compared to the neutral precursor, **PFN-Br**. The interfacial energy levels can be characterized using the experimentally

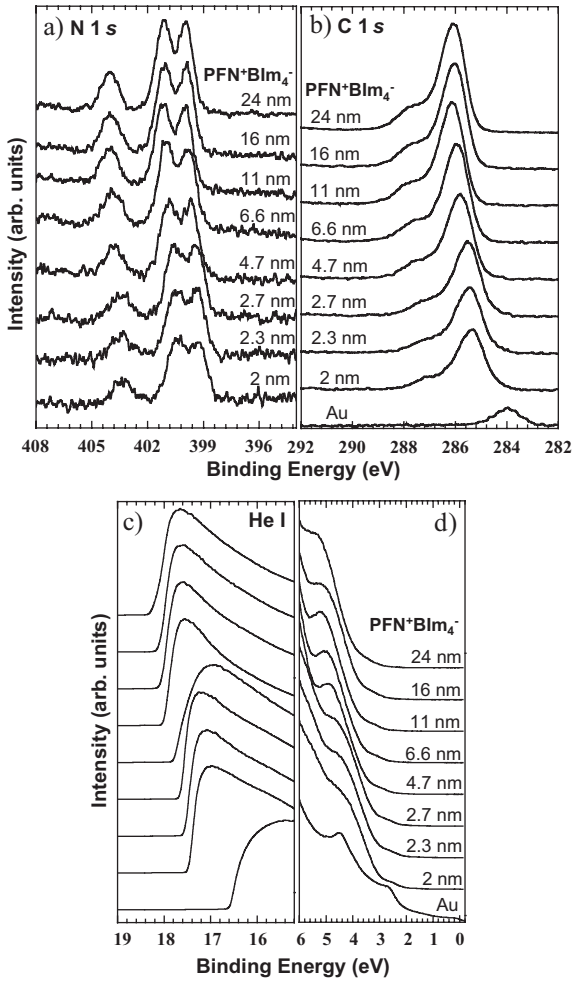

Figure 6. The XPS spectra of a) N 1s, and b) C 1s core levels of $PFN^+BIm_4^-$ films with increasing $PFN^+BIm_4^-$ thickness. UPS spectra of d) the secondary edge region and e) the HOMO region of $PFN^+BIm_4^-$ with increasing $PFN^+BIm_4^-$ thickness.

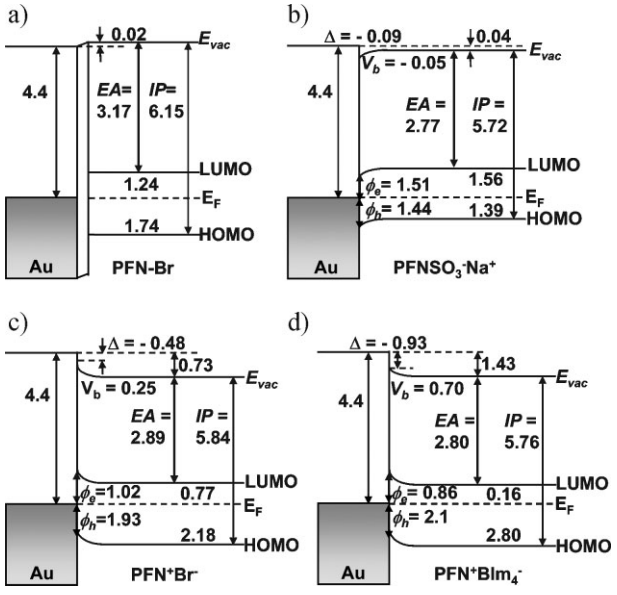

Figure 7. Energy level alignments of a) **PFN-Br**, b) $PFNSO_3^-Na^+$, c) PFN^+Br^-, and d) $PFN^+BIm_4^-$ interface. The energy unit is eV. (E_F: Fermi energy level, E_{vac}: VL, Δ: interfacial dipole, EA: electron affinity, IP: ionization potential, V_b: band bending, ϕ_e: electron injection barrier, ϕ_h: hole injection barrier).

determined ϕ_{Au}. It has already been known that the ϕ_{Au} of a thermally deposited Au surface is about 4.4–4.7 eV rather than 5.1–5.2 eV, a value typical for polycrystalline and atomically clean Au surfaces.[9a,15] For that reason, the four polymers exhibit IP values larger than 5 eV and an EA smaller than 3 eV; the E_F of Au exists somewhere within the polymer band gap. Hole (electron)-injection barriers can be estimated by the energy difference between E_F of Au and the HOMO (LUMO) levels. In Figure 7a, the ϕ_e of **PFN-Br** is lower than the ϕ_h. **PFN-Br** exhibits a higher IP (6.15 eV) than the anionic (5.72 eV) and cationic CPEs (5.84 eV for PFN^+Br^- and 5.76 eV for $PFN^+BIm_4^-$). No significant change of both Δ and band bending was detected for the neutral **PFN-Br**. This result indicates that the **PFN-Br**/Au interface is essentially dipole free. In other words, the electronic states of **PFN-Br** and Au align at the VL. $PFNSO_3^-Na^+$ would be anticipated to exhibit the lowest ϕ_h in Figure 7b. Little change in the core levels and secondary edges show that the interface forms without significant charge transfer, and there is no evidence of chemical reaction. Comparison of the diagram of $PFNSO_3^-Na^+$ against those of PFN^+Br^- and $PFN^+BIm_4^-$ shows that the cationic polymers have larger interfacial dipoles and band bending. The ϕ_e values of PFN^+Br^- and $PFN^+BIm_4^-$ are also lower by comparison with $PFNSO_3^-Na^+$, as determined by the downward VL shift. This shift is likely a combination of charge transfer with Au and alignment of polar functionalities at the interface.[8a,20]

In summary, we provide herein the first complete picture of the electronic features at a CPE/metal interface. A critical component of the study is the ability to control film thickness by adjusting spin-casting conditions. XPS and UPS measurements can therefore be carried out progressively further away from the metal surface. For the cationic polymers studied here, strong band bending and interfacial dipole are observed on gold surfaces. Such features are not observed in the case of the neutral **PFN-Br** and anionic $PFNSO_3^-Na^+$ counterparts. The absence of changes in the XPS spectra indicates the absence of chemical-bond formation between the CPEs and the Au surface. Previous studies by cyclic voltammetry determined that the HOMO and LUMO levels of CPEs are not influenced by the pendant ionic charges.[21] Herein, we show that this is not the case in the solid state. Comparison of the properties of $PFN^+BIm_4^-$ and PFN^+Br^- shows how critical properties of the semiconducting component can be modified by choice of counterion. The larger counterion (diameters: BIm_4^-, ~8.98 Å; Br^-, 3.92 Å) leads to a smaller IP value, larger interfacial dipole, and more-pronounced band bending. One clear implication of the collective set of observations is that peripheral structural modifications can be used to engineer either hole-injection or electron-injection layers with a constant backbone structure. These findings are important for understanding how these materials function in PLEDs, the improvement of device performance, and the design of new materials for use in polymer-based optoelectronic devices.

Experimental

Detailed synthetic methods for CPE synthesis are described in the literature [1a]. The polymer solutions were prepared in chlorobenzene for **PFN-Br**, a 2:1 mixture of methanol and water for **PFNSO$_3^-$Na$^+$**, and methanol for **PFN$^+$Br$^-$** and **PFN$^+$BIm$_4^-$** [1b,13b]. For XPS and UPS experiments, a Au film 75 nm thick was deposited on a precleaned Si substrate with a thin native oxide. Polymer solutions were then spin-coated at different spin speeds and concentrations from each solution, atop a Au film. The total time of spin coating was kept at 60 s for all samples. Film fabrication was done in a N_2-atmosphere globe box. To minimize possible influence by exposure to air, the films were then transferred from the N_2-atmosphere dry box to the analysis chamber inside an air-free holder. Subsequently, all samples were kept inside a high-vacuum chamber overnight, to remove solvent.

The XPS and UPS analysis chamber was equipped with a hemispherical electron-energy analyzer (Kratos Ultra Spectrometer), and was maintained at 1.33×10^{-7} Pa. The XPS was measured using monochromatized Al $K\alpha$ ($h\nu = 1486.6$ eV) excitation, while UPS measurements were carried out using the He I ($h\nu = 21.2$ eV) source. The electron energy analyzer was operated at constant pass energy of 20 eV (for XPS) and 10 eV (for UPS). During UPS measurements, a sample bias of -9 V was used in order to separate the sample and the secondary edge for the analyzer. In order to confirm reproducibility of XPS and UPS spectra, we repeated these measurements twice on two sets of samples.

Relative elemental analysis obtained from XPS peak intensities confirm greater than 95% correct composition for **PFN$^+$Br$^-$**, **PFN$^+$BIm$_4^-$**, and **PFNSO$_3^-$Na$^+$** (see Fig. S1 in the Supporting Information).

Acknowledgements

The authors thank the NSF (DMR 0547639 and DMR 0606414) for the financial support. Supporting Information is available online from Wiley InterScience or from the author.

Received: August 19, 2008
Revised: October 25, 2008
Published online: December 30, 2008

[1] a) R. Yang, H. Wu, Y. Cao, G. C. Bazan, *J. Am. Chem. Soc.* **2006**, *128*, 14422. b) A. Garcia, R. Yang, Y. Jin, B. Walker, T.-Q. Nguyen, *Appl. Phys. Lett.* **2007**, *91*, 153502.

[2] M. B. Ramey, J. Hiller, M. F. Rubner, C. Tan, K. S. Schanze, J. R. Reynolds, *Macromolecules* **2005**, *38*, 234.

[3] a) J. Yang, A. Garcia, T.-Q. Nguyen, *Appl. Phys. Lett.* **2007**, *90*, 103514. b) L. Ding, M. Jonforsen, L. S. Roman, M. R. Andersson, O. Inganäs, *Synth. Met.* **2000**, *110*, 133. c) P. Taranekar, Q. Qiao, H. Jiang, I. Ghiviriga, K. S. Schanze, J. R. Reynolds, *J. Am. Chem. Soc.* **2007**, *129*, 8958.

[4] a) M. R. Pinto, K. S. Schanze, *Proc. Natl. Acad. Sci. USA* **2004**, *101*, 7505. b) A. Satrijo, T. M. Swager, *J. Am. Chem. Soc.* **2007**, *129*, 16020. c) C. Y. Chi, A. Mikhailovsky, G. C. Bazan, *J. Am. Chem. Soc.* **2007**, *129*, 11134.

[5] a) R. H. Friend, R. W. Gymer, A. B. Holmes, J. H. Burroughes, R. N. Marks, C. Taliani, D. D. C. Bradley, D. A. D. Santos, J. L. Brédas, M. Lögdlund, W. R. Salaneck, *Nature* **1999**, *397*, 121. b) A. W. Grice, D. D. C. Bradley, M. T. Bernius, M. Inbasekaran, W. W. Wu, E. P. Woo, *Appl. Phys. Lett.* **1998**, *73*, 629.

[6] a) V. Cimrová, W. Schmidt, R. Rulkens, M. Schulze, W. Meyer, D. Neher, *Adv. Mater.* **1996**, *8*, 585. b) H. D. Burrows, M. Knaapila, A. P. Monkman, M. J. Tapia, S. M. Fonseca, M. L. Ramos, W. Pyckhout-Hintzen, S. Pradhan, U. Scherf, *J. Phys.: Condens. Matter.* **2008**, *20*, 104210.

[7] R. Yang, A. Garcia, D. Korystov, A. Mikhailovsky, G. C. Bazan, T.-Q. Nguyen, *J. Am. Chem. Soc.* **2006**, *128*, 16532.

[8] a) H. Ishii, K. Sugiyama, E. Ito, K. Seki, *Adv. Mater.* **1999**, *11*, 605. b) Y. Gao, *Acc. Chem. Res.* **1999**, *32*, 247. c) S. C. Veenstra, H. T. Jonkman, *J. Polym. Sci, Part B: Polym. Phys.* **2003**, *41*, 2549.

[9] a) W. Osikowicz, M. P. de Jong, S. Braun, C. Tengstedt, M. Fahlman, W. R. Salaneck, *Appl. Phys. Lett.* **2006**, *88*, 193504. b) I. H. Campbell, T. W. Hagler, D. L. Smith, J. P. Ferraris, *Phys. Rev. Lett.* **1996**, *76*, 1900. c) J. Hwang, E.-G. Kim, J. Liu, J.-L. Brèdas, A. Duggal, A. Kahn, *J. Phys. Chem. C* **2007**, *111*, 1378.

[10] a) J. H. Seo, T. M. Pedersen, G. S. Chang, A. Moewes, K.-H. Yoo, S. J. Cho, C. N. Whang, *J. Phys. Chem. B* **2007**, *111*, 9513. b) A. Gadisa, K. Tvingstedt, S. Admassie, L. Lindell, X. Crispin, M. R. Andersson, W. R. Salaneck, O. Inganäs, *Synth. Met.* **2006**, *156*, 1102.

[11] R. Schlaf, P. G. Schroeder, M. W. Nelson, B. A. Parkinson, P. A. Lee, K. W. Nebesny, N. R. Armstrong, *J. Appl. Phys.* **1999**, *86*, 1499.

[12] a) C. Shen, A. Kahn, *J. Appl. Phys.* **2001**, *90*, 4549. b) S. Braun, W. Osikowicz, Y. Wang, W. R. Salaneck, *Org. Electron.* **2007**, *8*, 14.

[13] a) N. Dam, M. M. Beerbom, J. C. Braunagel, R. Schlaf, *J. Appl. Phys.* **2005**, *97*, 024909. b) J. H. Seo, T.-Q. Nguyen, *J. Am. Chem. Soc.* **2008**, *130*, 10042.

[14] a) G. Greczynski, M. Fahlman, W. R. Salaneck, *J. Chem. Phys.* **2000**, *113*, 2407. b) C. Tengstedt, W. Osikowicz, W. R. Salaneck, I. D. Parker, C.-H. Hsu, M. Fahlman, *Appl. Phys. Lett.* **2006**, *88*, 053502.

[15] a) A. Wan, J. Hwang, F. Amy, A. Kahn, *Org. Electron.* **2005**, *6*, 47. b) J. E. Lyon, A. J. Cascio, M. M. Beerbom, R. Schlaf, Y. Zhu, S. A. Jenekhe, *Appl. Phys. Lett.* **2006**, *88*, 222109.

[16] a) R. Hauert, A. Glisenti, S. Metin, J. Goitia, J. H. Kaufman, P. H. M. van Loosdrecht, A. J. Kellock, P. Hoffmann, R. L. White, B. D. Hermsmeier, *Thin Solid Films* **1995**, *268*, 22. b) R. L. Graham, C. D. Bain, H. A. Biebuyck, P. E. Laibinis, G. M. Whitesides, *J. Phys. Chem.* **1993**, *97*, 9456.

[17] S. A. Al-Bataineh, L. G. Britcher, H. J. Griesser, *Surf. Interface Anal.* **2006**, *38*, 1512.

[18] a) E. Uchida, Y. Ikada, *J. Appl. Polym. Sci.* **1996**, *61*, 1365. b) L. Köhler, D. Gourdin, R. Sporken, K. Grigorov, J. Riga, R. Caudano, *Polym. Int.* **1998**, *47*, 474.

[19] a) J. Li, L. Vaisman, G. Marom, J.-K. Kim, *Carbon* **2007**, *45*, 744. b) I. V. Klimenko, T. S. Zhuravleva, V. M. Geskin, T. Jawhary, *Mater. Chem. Phys.* **1998**, *56*, 14.

[20] K. Seki, H. Yanagi, Y. Kobayashi, T. Ohta, T. Tani, *Phys. Rev. B* **1994**, *49*, 2760.

[21] Y. Zhang, Y. Xu, Q. Niu, J. Peng, W. Yang, X. Zhu, Y. Cao, *J. Mater. Chem.* **2007**, *17*, 992.